Analysis of cloud condensation nuclei properties at a polluted site in southeastern China during the AMF-China Campaign

Jianjun Liu,[1,2] Youfei Zheng,[1] Zhanqing Li,[1,2,3] and Maureen Cribb[2]

[1] Cloud condensation nuclei (CCN) measurements are essential to understanding cloud processes but CCN measurements are scarce. This study analyzes CCN measurements acquired at Shouxian, a polluted site in southeastern China, from August 1–October 31, 2008 during the deployment of the U.S. Department of Energy's (DOE) Atmospheric Radiation Measurement (ARM) Mobile Facility (AMF). The ranges of daily mean condensation nuclei concentrations (N_{CN}) were approximately 3100–12000, 2300–7400, and 4260–15500 cm^{-3} in August, September, and October, respectively; the corresponding ranges of CCN concentrations (N_{CCN}) at 0.49% supersaturation were about 1960–5670, 1770–3530, and 1500–5700 cm^{-3}. The average ratio of N_{CCN}/N_{CN} was 0.04, 0.12, 0.35, 0.53, 0.65, 0.69 and 0.72 for supersaturation values of 0.08%, 0.20%, 0.34%, 0.49%, 0.78%, 1.07% and 1.37%, respectively. N_{CN} and N_{CCN} peaked in the early morning and late afternoon, when human activities were most intense. CCN were more abundant in air masses influenced by anthropogenic pollution from densely populated areas. N_{CCN} was proportional to N_{CN}, but N_{CCN}/N_{CN} decreased with increasing N_{CN}. There was a good correlation between N_{CCN} (at 0.49% supersaturation) and aerosol optical depth (AOD) (500 nm), that is especially strong for fine-mode aerosols (Angstrom exponent (α) > 0.8). This relationship can be fitted with a power law function. The changes of N_{CCN} with various factors are explained. A dust event was identified showing a significant increase in N_{CN} and a dramatic decrease in the N_{CCN}/N_{CN} ratio, implying that dust particles do not increase N_{CCN} much, despite mixing with other anthropogenic aerosols.

1. Introduction

[2] Atmospheric aerosols play a significant role in global climate change by directly affecting Earth's radiative balance (direct effects) and indirectly altering cloud and precipitation properties (indirect effects). As a subset of atmospheric aerosols, cloud condensation nuclei (CCN) enable the condensation of water vapor to form cloud droplets. They are key elements in the hydrological cycle and climate on regional and global scales. Elevated CCN concentrations (N_{CCN}) cause an increase in the number of cloud droplets with a resultant decrease in cloud droplet average size [*Twomey*, 1974]. Determination of the spectrum of CCN and its spatial and temporal variations is a key challenge in quantifying aerosol indirect effects and is also essential to understanding the effects of CCN in meteorological models at all scales [*Huang et al.*, 2007].

[3] Many studies have been carried out regarding N_{CCN} at various locations, the relationship between CCN activity and aerosol size and chemical composition, and prediction of N_{CCN} using empirical relationships and model simulations [*Yum et al.*, 2005, 2007; *Rose et al.*, 2008; *Ross et al.*, 2003; *Khvorostyanov and Curry*, 2006; *Andreae*, 2009; *Kuang et al.*, 2009; *Oshima et al.*, 2009]. Due to their relatively short lifetimes, strong spatial and temporal variability and complex relations with the physical and chemical properties of aerosols, our knowledge of CCN and how they interact with aerosols, clouds, and ultimately climate is far from adequate. There is an urgent need to acquire more information about CCN and aerosols over major aerosol source regions, which play critical roles in global climate change.

[4] East Asia, especially the Yangtze River Delta region, is a fast developing and densely populated region, where anthropogenic emissions of aerosol particles and precursors have increased significantly over recent years [*Streets et al.*,

[1]Jiangsu Key Laboratory of Atmospheric Environment Monitoring and Pollution Control, Nanjing University of Information Science and Technology, Nanjing, China.
[2]Department of Atmospheric and Oceanic Science and Earth System Science Interdisciplinary Center, University of Maryland, College Park, Maryland, USA.
[3]State Key Laboratory of Earth Surface Processes and Resource Ecology, GCESS, Beijing Normal University, Beijing, China.
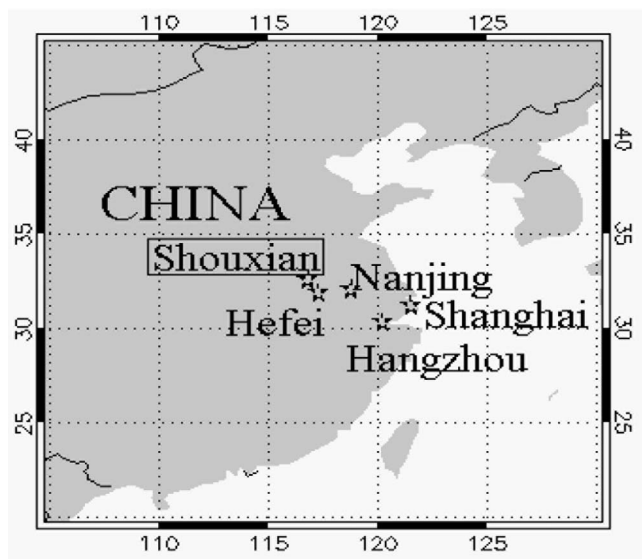
Figure 1. Location of the AMF Shouxian site in southeastern China and neighboring mega-cities.

2008] and where aerosol loading is high and aerosol composition is complex [*Li et al.*, 2007a, *Xin et al.*, 2007]. CCN generated here may affect clouds over extended areas of the western Pacific, as Asian pollution has been linked to intensification of storms downstream across the Pacific [*Zhang et al.*, 2007]. Numerous studies showed the significant influence of aerosols on radiative properties, cloud microphysics and precipitation in this part of the world [*Xu*, 2001; *Li et al.*, 2007b; *Xia et al.*, 2007; *Rosenfeld et al.*, 2007; *Lau et al.*, 2008]. So it is important to determine the spatial distribution of CCN and the relative contribution of CCN from anthropogenic sources. Only a handful of CCN measurements have been made in East Asia where mega-cities are likely to be major sources of pollutants and CCN [*Yum et al.*, 2007; *Rose et al.*, 2008; *Gunthe et al.*, 2009].

[5] From May to December 2008, extensive aerosol observations, as well as essential cloud, radiative, and meteorological variables for the study of aerosol indirect effects, were made during the Atmospheric Radiation Measurement (ARM) Program's mobile facility (AMF) deployment in China [*Li et al.*, 2011]. CCN and aerosol properties were characterized during the campaign. The aim of this paper is to study the general characteristics of N_{CCN} and its ratio to the proxy of total particle concentration (i.e., condensation nuclei, CN) at the site, laying a foundation for the investigation of the impact of aerosols on clouds and precipitation, a major objective of the campaign [*Li et al.*, 2011]. The dependence of CCN properties on meteorological conditions is analyzed. We also focus on the relationship between CCN and aerosol properties, including the relationship between N_{CCN} and N_{CN}, and aerosol optical properties and the effects of a moderate dust event on CCN properties observed during the observation period.

[6] The paper is organized as follows. The sampling site, instrumentation and data are described in the following section. Section 3 presents the results and discussion of the characteristics of CCN number concentrations and their activation properties, as well as the relationship between CCN properties and meteorological conditions. The relationship between CCN properties and N_{CN}, aerosol optical properties and CCN properties during a moderate dust event are also discussed in this section. The summary is presented in section 4.

2. Observation Site, Instruments and Data

2.1. Site Description

[7] With the goal of better understanding aerosol climate effects in China, and in particular, the interaction between aerosols, clouds and precipitation, the AMF was deployed in Shouxian, China, from May to December 2008 [*Li et al.*, 2011]. The site is located at the edge of a small town (population of approximately 70,000) and is largely surrounded by farmland in the Jiang-Huai prairie region between the Huai and Yangzi rivers. There are several big cities in the Yangtze Delta region surrounding the site (see Figure 1), including Shanghai (~500 km away), Nanjing (~200 km away), and Hefei (~100 km away). The climate of the region is subtropical and is affected by different air masses, such as maritime air masses to the east and continental air masses to the northwest. Several national and international meteorological experiments were conducted at the site, e.g., the Huaihe River Basin Energy and Water Cycle Experiment (HUBEX) under the aegis of the GEWEX-Asian Monsoon Experiment (GAME), and the Lower Atmosphere and Precipitation Study (LAPS).

2.2. Cloud Condensation Nuclei

[8] N_{CN} and N_{CCN} were measured by the ARM Aerosol Observation System which is the primary platform used for collecting in situ aerosol measurements at the surface [*Jefferson*, 2005]. CN were measured by the TSI model 3010 particle counter (CPC), which is a compact and rugged instrument that counts the number of particles greater than 10 nm in diameter. This is done by increasing the saturation ratio up to several hundred percent, so that aerosol particles are activated and grow big enough to be counted. The CPC has a high signal-to-noise ratio that limits false background counts to nearly zero, making detection of small particles remarkably accurate. Given that the upper concentration limit of the CPC is 10,000 particles per cubic centimeter and high particle concentrations were encountered at the observation site, an air sample dilution system was used. Particle concentrations were then multiplied by the dilution factor to obtain actual concentrations. The instrument responds quickly to concentration changes, showing readings in a matter of seconds. In this study, the sampling interval is 1 min. CCN is measured by the Droplet Measurement Technology (DMT) continuous flow CCN counter [*Roberts and Nenes*, 2005]. The instrument is calibrated annually or as needed if it shows poor performance. Calibration was done with ammonium sulfate aerosols as discussed by *Rissman et al.* [2006]. The CCN data were obtained by changing the supersaturation (SS) about every 5 min in 7 intervals (0.08%, 0.20%, 0.34%, 0.49%, 0.78%, 1.07% and 1.37%). Here, we used CCN data collected from August to October only because the instrument malfunctioned after November 1.
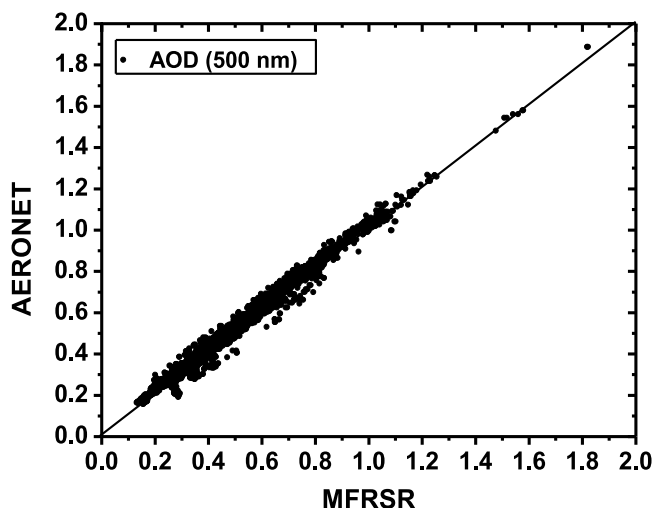
Figure 2. AERONET AOD at 500 nm as a function of MFRSR AOD.

2.3. Aerosol Optical Properties

[9] Aerosol optical properties were derived from measurements made by a CIMEL Sun/sky sunphotometer and a MultiFilter Rotating Shadow-band Radiometer (MFRSR). The CIMEL instrument, part of the worldwide Aerosol Robotic Network (AERONET), takes direct measurements of Sun and sky radiances at seven wavelengths (340, 380, 440, 500, 670, 870 and 1020 nm) from which spectral aerosol optical depths (AOD) are retrieved with an uncertainty of 0.01–0.02 [*Eck et al.*, 1999]. Under certain constraints, aerosol size distributions and single scattering albedos were also retrieved following the methodology of *Dubovik and King* [2000].

[10] The MFRSR is a seven-channel pyranometer with a rotating shadow band that measures total and diffuse irradiances at 415, 500, 610, 673, 870, and 940 nm, as well as total solar broadband irradiances, at 20-s intervals throughout the day [*Harrison and Michalsky*, 1994]. AOD can be retrieved using methods such as those described by *Alexandrov et al.* [2008] and *Lee et al.* [2010] with a typical measurement accuracy of 0.01 in AOD. Partitioning of spectral AODs into fine and coarse mode AODs and retrievals of the fine mode effective radius are possible. Cloud screening is based on the local variability of optical depth derived from direct-beam measurements at 870 nm [*Alexandrov et al.*, 2004]. Figure 2 shows a comparison of AODs at 500 nm retrieved from AERONET and MFRSR measurements. The two sets of retrievals agree very well. Both aerosol data sets are used to study the relationship between CCN and aerosol optical properties in order to increase the number of samples.

2.4. Aerosol Vertical Structure

[11] The aerosol vertical distribution was measured by a micropulse lidar (MPL), which is an elastic backscatter lidar developed at the NASA Goddard Space Flight Center and manufactured by the Sigma Space Corporation, United States. At the time of its deployment, the MPL operated at the 527-nm wavelength, and the laser pulse duration was

about 10 nsec with a pulse frequency of 2500 Hz. Given its pulsed solid-state laser, narrow field of view (~100 μrad), narrow interference filters (~0.3 nm FWHM), and photon counting detection capability, the MPL is a highly sensitive instrument. In this study, continuous aerosol and cloud measurements were acquired using a 30-m range resolution and a 1-min time average [*Campbell et al.*, 2002; *Welton et al.*, 2002].

[12] In the MPL system, one actively controlled liquid crystal retarder conducts polarization-sensitive measurements by alternately transmitting linearly and circularly polarized light. Using these two-mode measurements, the linear depolarization ratio can be estimated. Details regarding polarization sensitive lidar measurements and the calculation of the linear depolarization ratio are given by *Flynn et al.* [2007]. The linear depolarization ratio is an indicator of the extent of non-sphericity and is used as a tool for identifying and investigating dust aerosols, in addition to studying aerosol vertical distributions.

3. Results

3.1. Variation of N_{CN} and N_{CCN}

3.1.1. Daily and Diurnal Variations

[13] The mean AOD measured during the AMF campaign at Shouxian was 0.85 and varied considerably from day to day [*Lee et al.*, 2010]. The site is affected by dust, industrial pollutants and smoke with complex properties, complicating our understanding of the variation of CCN. Figure 3 shows the daily averaged values of N_{CN} (Figure 3, top) and N_{CCN} (Figure 3, middle) at 0.49% SS during the course of the field campaign. The letters O, S, T, and F along the top designate air mass types I, II, III and IV (see section 3.1.2 and Figure 6), respectively, during each day. Days when precipitation occurred are labeled with the letter R. Because the weather (clear, cloudy or rainy) on each day varied over time, it is difficult to classify specific weather patterns for each day. Significant temporal variations are seen, with daily averaged N_{CN} ranging from 3095 to 12014 cm^{-3} (August), 2315–7416 cm^{-3} (September), and 4267–15508 cm^{-3} (October) and daily averaged N_{CCN} ranging from 1964 to 5677 cm^{-3} (August), 1771–3536 cm^{-3} (September), and 1526–5706 cm^{-3} (October). Their diurnal variations are denoted by standard deviations (SD) shown as vertical lines protruding from the tops of the bars. The SD is very large in general and comparable to the day-to-day mean variations. N_{CN} during August and September is significantly smaller than in October, with monthly mean and SD values of 6444 ± 2732 cm^{-3} (August), 4644 ± 2454 cm^{-3} (September), and 9804 ± 4142 cm^{-3} (October). This variation is consistent with the variation in aerosol scattering coefficients measured by a nephelometer during the field campaign [*Fan et al.*, 2010]. Minimum values of N_{CCN} at 0.49% SS occurred in September (2475 ± 955 cm^{-3}), corresponding to the smallest values of N_{CN} during this month. However, the monthly mean N_{CCN} in August (3445 ± 1158 cm^{-3}) is larger than that in October (3178 ± 1269 cm^{-3}), which indicates that many more aerosols were not CCN in October. The number concentration of aerosol particles and the fraction of CCN active particles determine N_{CCN}. This fraction is often denoted as N_{CCN}/N_{CN} because condensation nuclei counters are used for total particle number concentration measure-

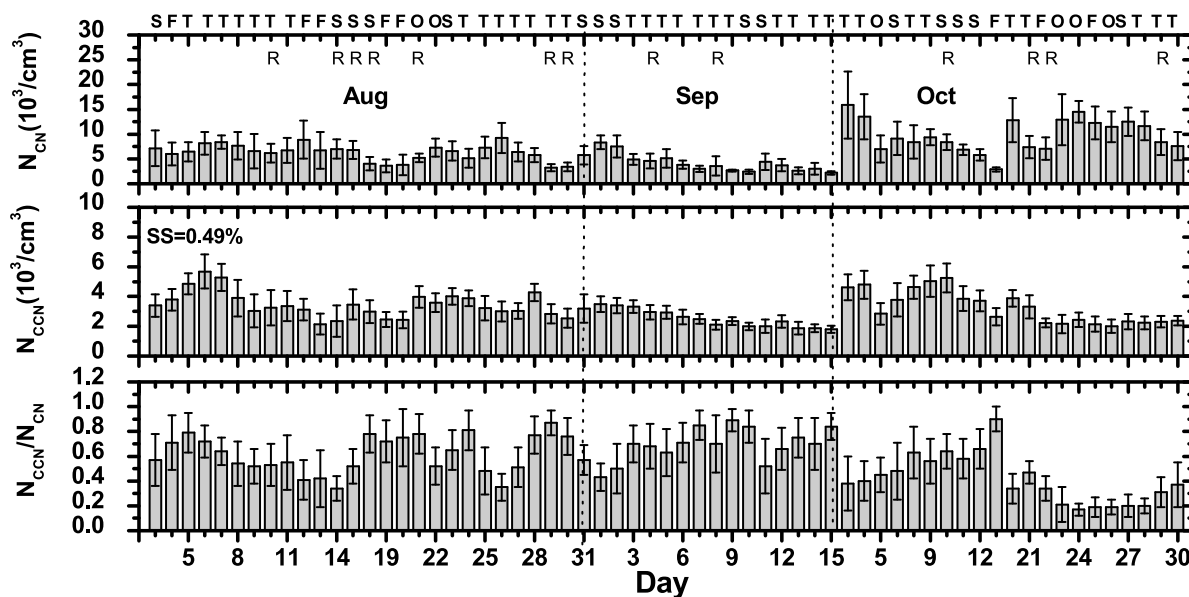**Figure 3.** Daily averaged values of (top) N_{CN}, (middle) N_{CCN} and (bottom) N_{CCN}/N_{CN} at 0.49% SS during the observation period. Shaded bars represent the mean values of N_{CN}, N_{CCN} and N_{CCN}/N_{CN}; vertical lines protruding from the top of the bars represent the standard deviation. The letters O, S, T, and F along the top designate air mass types I, II, III and IV (see Figure 6), respectively, during each day. The letter R indicates that precipitation occurred during the day.

ments. The daily mean values of N_{CCN}/N_{CN} from August to October are also plotted in Figure 3 (bottom). Large day-to-day variations in N_{CCN}/N_{CN} are seen during the campaign, ranging from 0.34 to 0.87 (August: mean = 0.600 ± 0.215), 0.43–0.89 (September: mean = 0.601 ± 0.245) and 0.17–0.90 (October: mean = 0.383 ± 0.207) at 0.49% SS. Larger values of N_{CCN}/N_{CN} are found in August and September, indicating that many more aerosol particles were activated as CCN during these two months than in October.

[14] Up until now, very limited CCN measurements have been made in Asia, especially in East China; some CCN measurements are summarized in Table 1. Mean N_{CN} and N_{CCN} during the whole period of our study are much higher than those measured during the Indian Ocean Experiment [*Hudson and Yum*, 2002], but are very similar to those measured at the Korea Global Atmosphere Watch Observatory on the west coast of the Korean Peninsula [*Yum et al.*, 2005] and at Gosan, Korea [*Yum et al.*, 2007]. The concentration of CCN measured at Shouxian is much lower than that measured during the PRIDE-PRD2006 campaign which took place at a rural site ~60 km northwest of the mega-city Guangzhou in southeastern China [*Rose et al.*, 2008], as well as that measured in the Guangzhou region and in Beijing [*Andreae*, 2009]. The average value of N_{CCN}/N_{CN} during the field campaign was 0.04, 0.12, 0.35, 0.53, 0.65, 0.69 and 0.72 for SS values of 0.08%, 0.20%, 0.34%, 0.49%, 0.78%, 1.07% and 1.37%, respectively, which is slightly larger than that reported in Beijing (0.44 at 0.4% SS) [*Andreae*, 2009] but similar to that measured near the Guangzhou region in southern China (0.49 at 0.4% SS) [*Andreae*, 2009]. A study by *Rose et al.* [2008] reported that N_{CCN}/N_{CN} ranged from 0.36 to 0.53 at SS = 0.27–0.47% at a rural site near Guangzhou city, which is similar to our results.

[15] Figure 4 shows the mean diurnal cycles of N_{CN} (Figure 4a), N_{CCN} (Figure 4b) and N_{CCN}/N_{CN} (Figure 4c) at 0.49% SS during the field campaign. Peaks in N_{CN} and N_{CCN} occurred in the early morning and in the late afternoon. They are probably related to human activities, such as emissions from traffic and cooking, which are most intense at these times of the day. As the convective boundary layer evolves during the late morning hours, cleaner air from aloft is mixed with pollutants near the surface, lowering the particulate concentration. Although N_{CCN} does not show any significant diurnal variation, small variations in N_{CCN} were found (subplot in Figure 4b). The change in N_{CN} and small variations in N_{CCN} are generally in phase, but the time at which peak values in N_{CCN} occur is about two hours behind that of N_{CN} in the morning and about one hour behind in the afternoon. This suggests that the newly formed small anthropogenic particles are inefficient as CCN because of their size limitation [*Dusek et al.*, 2006; *Yum et al.*, 2007]. This is consistent with the diurnal cycle of N_{CCN}/N_{CN}, where small values occur in the early morning and late afternoon and the largest values are seen around noon.

3.1.2. Variation With Meteorological Parameters

[16] During the field campaign, surface meteorology parameters were measured by the ARM Mobile Facility Surface Meteorology Station (AMFMET) at 1-min intervals. Measurements include surface wind speed, wind direction, air temperature, relative humidity, barometric pressure, and rain rate (http://www.arm.gov/instruments/met). The CCN distribution and activation efficiency of aerosols generally depend on particle size and chemical composition. It is well known that meteorological conditions can significantly influence aerosol chemistry [*Elminir*, 2005], size distribution [*Nicolás et al.*, 2009], sources,

Table 1. Summary of Results From Studies Made in East Asia Regarding Cloud Condensation Nuclei Properties Under 0.4% SS Conditions[a]

Region/Time	N_{CN} (cm^{-3})	N_{CCN} (cm^{-3})	N_{CCN}/N_{CN}	Comment	Location	Reference
			Polluted Marine			
Indian Ocean, NH Feb/Mar, 1999	1810 ± 40	1100 ± 100	0.61	INDOEX[b]	~0–4 N, ~72–74 E	*Hudson and Yum* [2002]
Anmyeon Isl., KR 1–22 May, 2004	3980 ± 970	1670 ± 390	0.42	Amnyon	36.54 N, 126.33 E	*Yum et al.* [2005]
Gosan, Korea 11 May–9 Apr, 2005	3510 ± 1790	1570 ± 500	0.45	ABC-EAREX[c]	33.29 N, 126.16 E	*Yum et al.* [2007]
			Polluted Continental			
Anmyeon Isl., KR 1–22 May, 2004	8310 ± 1780	3350 ± 980	0.40	Amnyon	36.54 N, 126.33 E	*Yum et al.* [2005]
Gosan, Korea 11 May–9 Apr, 2005	5600 ± 3500	2010 ± 950	0.36	ABC-EAREX	33.29 N, 126.16 E	*Yum et al.* [2007]
Guangdong rural Jul 2006	18700 ± 8200	9100 ± 4800	0.44	PRIDE-PRD 2006[d]	23.49 N, 113.04 E	*Rose et al.* [2008]
Guangzhou region Sep–Oct 2004	16500 ± 8800	7300 ± 3300	0.44	CN > 60 nm Xinken site	22.60 N, 113.60 E	A. Wiedensohler[a]
Beijing, 10 Aug–9 Sep, 2006	16200 ± 8500	7200 ± 3000	0.44	Yufa site	39.52 N, 116.33 E	D. Rose, unpublished[a]

[a]From *Andreae* [2009].
[b]Indian Ocean Experiment.
[c]Atmospheric Brown Clouds–East Asian Regional Experiment.
[d]Program of Regional Integrated Experiments of Air Quality over the Pearl River Delta.

transport and diffusion of particles [*Elminir*, 2005], and their optical properties [*Cheng et al.*, 2008]. Changes in particle properties affect CCN properties, such as concentration, size distribution and the activation efficiency. Here, we present observed results regarding the potential dependence of N_{CCN} and particle activation efficiency on a few key meteorological variables.

3.1.2.1. Ambient Temperature

[17] Figure 5 shows mean N_{CN} (Figure 5a), N_{CCN} (Figure 5b) and N_{CCN}/N_{CN} (Figure 5c) at 0.20% and 0.49% SS as a function of ambient temperature during the field campaign. The values of N_{CN}, N_{CCN} and N_{CCN}/N_{CN} were averaged over every 1°C temperature bin. N_{CN} decreases significantly when the temperature increases from around 9°C to about 21°C then remains fairly constant at temperatures greater than 21°C. Note that temperature is a key weather index that experiences large changes with the seasons, as does the air mass. The higher concentration of CN at lower temperatures are most likely coarse aerosols carried in by an air mass originating from the northwestern part of China (described in a later section). Both N_{CCN} and N_{CCN}/N_{CN} increase with increasing temperature. One reason for this dependency is that during the late summer and early fall, temperatures are high and the dominant summer monsoon circulation ushers in an air mass originating over the ocean to the east. Because marine aerosols are expected to be more soluble than aerosols of a continental origin [*Hudson and Da*, 1996], CCN activation for marine aerosols

should be higher than that of continental aerosols. Another possible reason for the increase in CCN with increasing temperature may be related to photochemical reactions and/or particle growth. Changes in temperature can shift the phase partitioning between gaseous and aqueous aerosol states. For example, N_{CN} decreases with increasing temperature as volatile aerosols vaporize until the volatile aerosol population is largely exhausted (Figure 5a). At this point N_{CN} remains fairly stable with increasing temperature. N_{CCN} increases with increasing temperature as vaporized aerosol species re-condense on larger aerosol particles, creating a soluble surface layer. If warmer temperatures are associated with more clear atmospheric conditions, perhaps additional photochemical reactions yielding more secondary aerosols will occur. In other words, the dependence of CCN on temperature may be a true phenomenon, or just a manifestation of another real cause for which temperature is a proxy.

[18] A decrease in CCN with increasing temperature was reported by *Saleeby and Cotton* [2004]. However, their result does not conflict with ours. Using the Lagrangian parcel model approach, the parcel considered in their study was lifted to a point where maximum supersaturation was achieved; the fraction of CCN that are activated should be greater at warmer temperatures in the case of stationary growth [*Saleeby and Cotton*, 2004]. It is worth noting that our analysis does not address the question of the intrinsic dependence of CCN properties on temperature, which is not
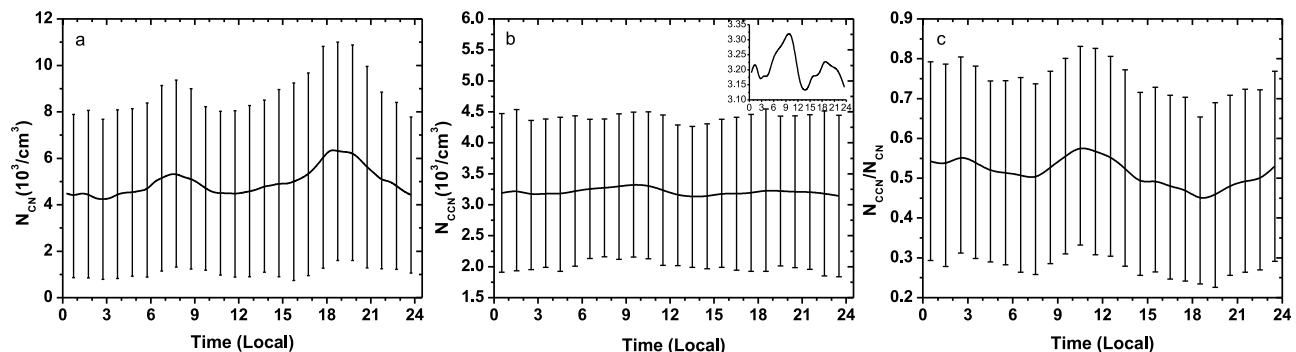
Figure 4. Diurnal cycle of mean (a) N_{CN}, (b) N_{CCN} and (c) N_{CCN}/N_{CN} at 0.49% SS during the observation period. Vertical bars represent the standard deviation.
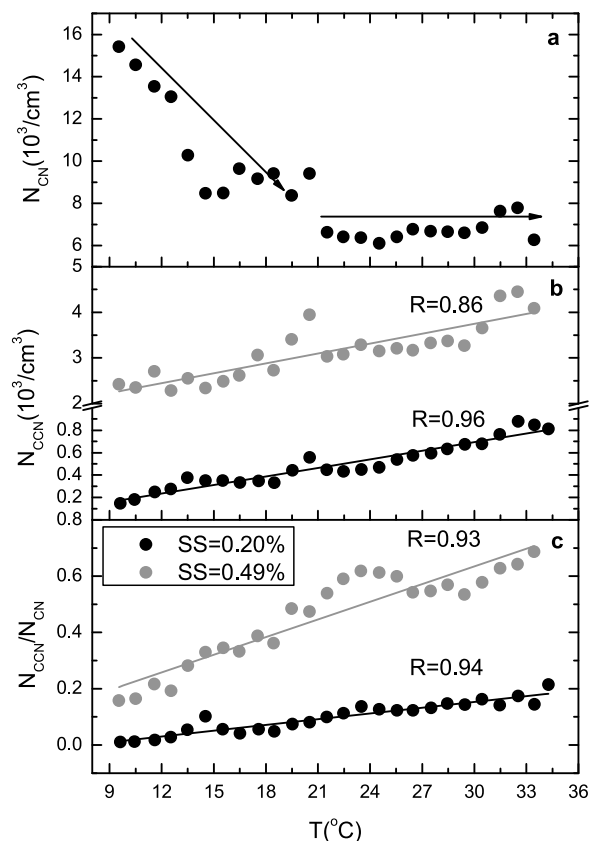
Figure 5. Mean (a) N_{CN}, (b) N_{CCN} and (c) N_{CCN}/N_{CN} at 0.2% and 0.49% SS as a function of ambient temperature during the observation period. N_{CN}, N_{CCN} and N_{CCN}/N_{CN} are averaged over every 1°C temperature bin from the lowest temperature to the highest temperature.

yet well understood. The temperature dependence of CCN reported here is probably intermingled with the factors stated above.

3.1.2.2. Air Mass

[19] The dominant aerosol type over an area largely depends on the air mass over the area. Back-trajectory analysis is performed to discuss the potential effects of air mass on CCN properties at Shouxian using the HYbrid Single-Particle Lagrangian Integrated Trajectory (HYSPLIT) model with the Global Data Assimilation System (GDAS1) meteorological database (R. R. Draxler and G. D. Rolph, HYSPLIT (HYbrid Single-Particle Lagrangian Integrated Trajectory) Model, 2010, http://ready.arl.noaa.gov/HYSPLIT.php). All 3-day back trajectories at 500 m above ground level (AGL) on all observation days were calculated and four major types of air masses were identified during the course of the field campaign (see Figure 6). The Type I air mass originated from a remote area in the continental northwestern part of China and moved directly from the northwest to the Shouxian site. This remote part of China is rich with coarse aerosols, which consist of dust intermingled with pollution as the air mass traveled eastward. The Type II air mass originated from northeastern China, which is a highly industrialized part of the country with high levels of anthropogenic pollution. Marine and continental pollution aerosols are the dominant aerosol components of the Type

III air mass, which originated over the ocean to the east of Shouxian. The Type IV air mass is characterized by continental pollution from the more southerly parts of China. During the study period, the occurrence of Type I, II, III and IV air masses was 9%, 24%, 54% and 13%, respectively.

[20] Table 2 lists the mean N_{CN}, N_{CCN} and N_{CCN}/N_{CN} for each air mass type. The Type I air mass has the highest value of N_{CN} (9492 ± 4332 cm^{-3}) and lowest value of N_{CCN} (2708 ± 4887 cm^{-3}) while the other air mass types have roughly the same N_{CN} and N_{CCN}. N_{CCN} is higher in Types II, III, and IV air masses than in the Type I air mass. This indicates that CCN are more abundant in air masses that are influenced by anthropogenic pollution from densely populated areas. This is consistent with the results from a study made by *Yum et al.* [2007] based on measurements from Gosan, Korea. The small value of N_{CCN}/N_{CN} for the Type I air mass is likely due to the weak hygroscopicity of dust particles. *Rose et al.* [2008] showed that differences in CCN activation depended significantly on aerosol chemical composition and especially on hygroscopicity.

[21] As mentioned above, the Type III air mass originated over the sea, but is affected by anthropogenic pollutants so may be classified as an anthropogenically modified maritime air mass. Thus air masses are broadly classified as continental (Type I + Type II + Type IV) and anthropogenically modified maritime (Type III) in this study. Differences in CCN properties between these two air masses were examined. The magnitude of N_{CN} is similar for both continental and anthropogenically modified maritime air masses (7777 ± 3790 cm^{-3} and 7384 ± 3969 cm^{-3}, respectively). N_{CCN}/N_{CN} is larger in the polluted maritime air mass (0.56 ± 0.23 at 0.49% SS) than in the continental air mass (0.48 ± 0.24 at 0.49% SS) because marine aerosols are expected to be more soluble than aerosols of continental origin [*Hudson and Da*, 1996]. This results in a slightly larger N_{CCN} in the anthropogenically modified maritime air mass than in the continental air mass since the magnitude of N_{CN} is similar between them. A study over the west coast of Korea showed that N_{CN} and N_{CCN} are significantly greater
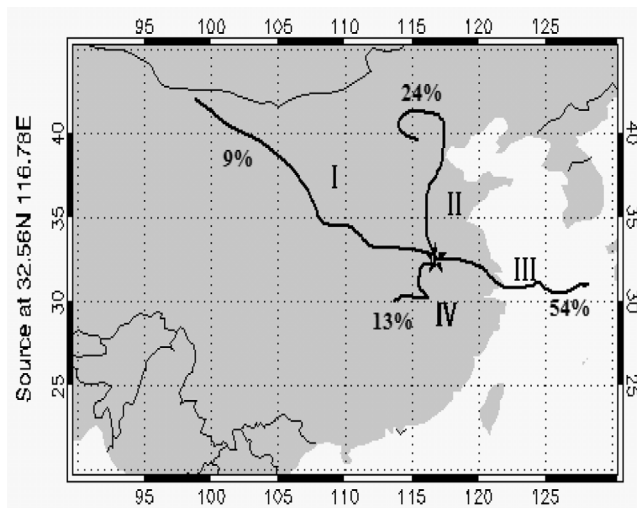

Figure 6. Four air mass types identified based on 6-hourly 3-day air mass back trajectories at 500 m above ground level during the observation period.

Table 2. Mean N_{CN} (1/cm^3), N_{CCN} (1/cm^3) and N_{CCN}/N_{CN} at 0.49% SS for Types I–IV Air Masses and for the Continental Air Mass (Type I + Type II + Type IV)

	I	II	III	IV	Continental
N_{CN}	9492 ± 4332	7170 ± 3020	7384 ± 3969	7185 ± 4016	7777 ± 3790
N_{CCN}	2708 ± 887	3330 ± 1128	3491 ± 1313	3207 ± 826	2992 ± 1056
N_{CCN}/N_{CN}	0.36 ± 0.23	0.53 ± 0.22	0.56 ± 0.23	0.49 ± 0.27	0.48 ± 0.24

in continental air masses than in maritime air masses and that the mean ratio of N_{CCN} and N_{CN} are similar in both air masses [*Yum et al.*, 2005]. This difference from our study suggests that by the time the marine air mass reached Shouxian, an abundant amount of continental pollution had been mixed in.

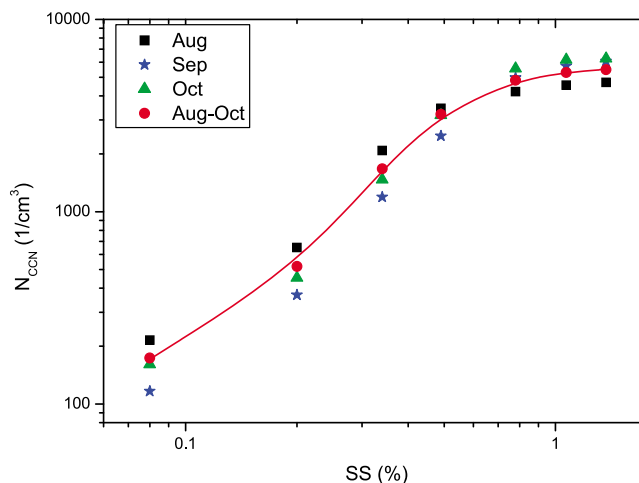### 3.1.3. N_{CCN} as a Function of SS

[22] The Twomey formula is the most widely used parameterization for determining the number of CCN (N) as a power law function of supersaturation (S), namely, N = CS^k, where the coefficients C and k are parameters related to particle concentration and chemical composition [*Martins et al.*, 2009]. However, it overestimates N_{CCN} at large SS and predicts unconstrained CCN with increasing total aerosol concentration. So a modified Twomey model was proposed and used in models which predict finite N_{CCN} at high SS limited by N_{CN} [*Ghana et al.*, 1995; *Abdul-Razzak and Ghan*, 2000; *Cohard et al.*, 2000; *Fountoukis and Nenes*, 2005; *Khvorostyanov and Curry*, 2006, 2007, 2008, 2009]. Figure 7 shows the monthly mean and total mean (over the entire period) N_{CCN} as a function of SS during our study. It illustrates how a straight line in log-log coordinates does not fit well the actual CCN activity spectra at high SS; C and k are not constant, but decrease with increasing SS [*Yum and Hudson*, 2001]. These decreasing functions of C and k could be described more precisely if the parameters of aerosol lognormal size spectra (modal radii and dispersions) and physicochemical properties were known using a new power law formulation proposed by *Khvorostyanov and Curry* [2006]. As a test, we fitted the N_{CCN} activity spectra during the entire period based on the method of *Khvorostyanov and Curry* [2006]. Initial values of the modal radius and dispersion were 0.045 μm and 2.15, respectively, which are typical values for aerosol particles in the accumulation mode [*Khvorostyanov and Curry*, 2006]. An additional assumption is that aerosols possessed volume-proportional soluble components (0.5) consisting of 50% ammonium sulphate or 20% NaCl. Modal radii and dispersions were tuned slightly in the calculations to provide the best agreement for both k(SS) and N_{CCN}(SS) over the entire range of SS. Details regarding C and k were calculated for different SS are given by *Khvorostyanov and Curry* [2006]. The calculated k decreases significantly with increasing SS, changing from 0.66 at SS = 0.08% to 0.05 at SS = 1.37%. It is clear that we need real aerosol physical-chemical properties to properly fit CCN spectra, which are generally not available [*Martins et al.*, 2009].

3.2. CCN and Aerosol Properties

[23] The CCN concentration depends significantly on the aerosol particle size distribution and chemical composition. N_{CCN} can be predicted on the basis of these parameters according to Köhler theory [*Rose et al.*, 2008; *Asa-Awuku et al.*, 2009].

3.2.1. CCN as a Function of CN

[24] Figure 8 shows the scatterplots of N_{CCN} (Figure 8, left) and N_{CCN}/N_{CN} (Figure 8, right) as a function of N_{CN} (integrated over every 0.5 * 10^3/cm^3 bin), as well as fitted power law functions for specific values of SS. Vertical bars represent standard deviations. N_{CCN} increases with increasing N_{CN} under all SS conditions and the correlation increases as SS increases. The correlation coefficients (R^2) at 0.2%, 0.49% and 1.07% SS are 0.48, 0.76 and 0.95, respectively. Different features are seen in the variation of N_{CCN}/N_{CN} with increasing N_{CN} as SS changes. When SS is less than 0.49%, N_{CCN}/N_{CN} tends to decrease with increasing N_{CN}; when SS is greater than 0.78%, N_{CCN}/N_{CN} tends to increase with increasing N_{CN}. The same behavior was seen in measurements from Gosan, Korea, which showed that at 0.6% SS, N_{CCN} increased with N_{CN} but N_{CCN}/N_{CN} decreased [*Yum et al.*, 2007]. An increase in N_{CN} could increase the number of particles within the activation size range or increase the number of particles that are too small for activation or both. The ratio N_{CCN}/N_{CN} decreases with N_{CN} because a greater number of particles were CCN inactive when N_{CN} was higher, which is likely due to a greater number of smaller particles present and/or their chemical composition was less favorable for activating as CCN. Smaller particles have higher critical supersaturations [*Dusek et al.*, 2006]. When SS is high, larger particles are activated as CCN [*Rose et al.*, 2008], leading to an increase in N_{CCN}/N_{CN}. The standard deviations are relatively large which indicates that there is much variation in N_{CCN} for a given N_{CN}. This makes it difficult to estimate CCN con-

Figure 7. Monthly averaged N_{CCN} as a function of SS. The red line is the best fit line calculated using the parameterization of *Khvorostyanov and Curry* [2006] with an assumed aerosol modal radius of 0.045 μm and a dispersion of 2.15.
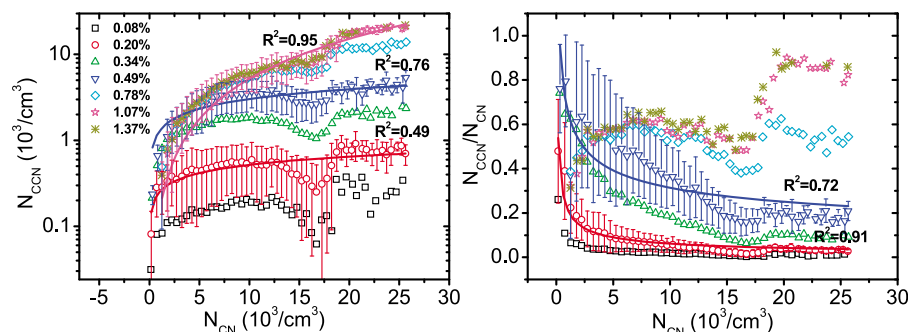
Figure 8. (left) N_{CCN} and (right) N_{CCN}/N_{CN} at different supersaturation levels as a function of N_{CN}, which is integrated over every $0.5 * 10^3/cm^3$ bin. The vertical bars represent the standard deviation. Power law fits are shown as solid lines.

centrations under polluted conditions without any knowledge of physical and chemical properties [*Yum et al.*, 2007].

[25] A modified power law function of the form $N_{ccn,s} = N_{cn,30} \cdot S^{-q}$ (where $N_{cn,30}$ stands for N_{CN} for particles with diameters greater than 30 nm, $S = 1 + SS/(100\%)$ and q is a parameter related to chemical composition) was used to describe the relationship between N_{CCN} and $N_{cn,30}$ in the studies of *Rose et al.* [2008] and *Gunthe et al.* [2009]. Their results showed that at high supersaturations ($SS > 0.47\%$), $N_{CCN,S}$ is closely correlated to $N_{CN,30}$ ($R^2 = 0.80$–0.98), and that the mean relative deviations between the power law fit and the measured values of $N_{CCN,S}$ were only 4–27%. At a lower SS, for example, when $SS = 0.27\%$, the correlation is much worse ($R^2 = 0.61$, mean deviation = 40%) [*Rose et al.*, 2008; *Gunthe et al.*, 2009].

3.2.2. CCN as a Function of Aerosol Optical Properties

[26] Because of the high cost and complexity of operation, in situ measurements of N_{CCN} are rare and may not represent large areas. On the other hand, AOD is more readily observed by both ground-based and space-borne sensors. Using a large number of published and unpublished measurements of N_{CCN} at 0.4% SS and AOD at 500 nm, *Andreae* [2009] found a general relation between the two quantities that was expressed as a power law function: $N_{CCN0.4} = 10316 \cdot [AOD_{500}]^{1.56}$. The relationship was derived from measurements acquired under a variety of environments: remote marine, remote continental, polluted marine and polluted continental. Figure 9a shows mean N_{CCN} (at $SS = 0.49\%$) as a function of AOD (500 nm) at

Shouxian. Near-simultaneous measurements of N_{CCN} and AOD were made and N_{CCN} values were averaged over each 0.1 AOD bin. Despite large variations, as illustrated by the standard deviations, there is a reasonable relationship between mean N_{CCN} and AOD ($R^2 = 0.64$).

[27] Note that CCN is primarily influenced by fine-mode aerosols [*Andreae*, 2009]. *Andreae* [2009] suggested a correlation between CCN and the Ångstrom exponent (α), which contains aerosol size information. The black line in Figure 9b is the best fit line through simultaneous measurements of N_{CCN} as a function of α during the field campaign. The potential relationship between CCN and fine-mode aerosols was examined using only measurements with $\alpha > 0.8$ (red line). A good correlation was found during the entire period ($R^2 = 0.66$), and was especially strong for fine-mode aerosols ($R^2 = 0.84$). A larger Ångstrom exponent implies a smaller particle size. So the positive relationship between N_{CCN} and α suggests that N_{CCN} increased as particle size decreased. This seems counterintuitive. An explanation may be that there is no significant decrease in the portion of aerosol particles within the activation size range with increasing α, and/or there is an increase in the portion of particles with chemical compositions more favorable for activation as CCN. This is compelling, given that different types of aerosols do have systematic discrepancies in their particle sizes, e.g., coarse-mode dust versus fine-mode anthropogenic pollutants. The former is much less hygroscopic than the latter.

[28] We also examined the relationship between CCN and both AOD and α as proposed by *Nakajima et al.* [2001].
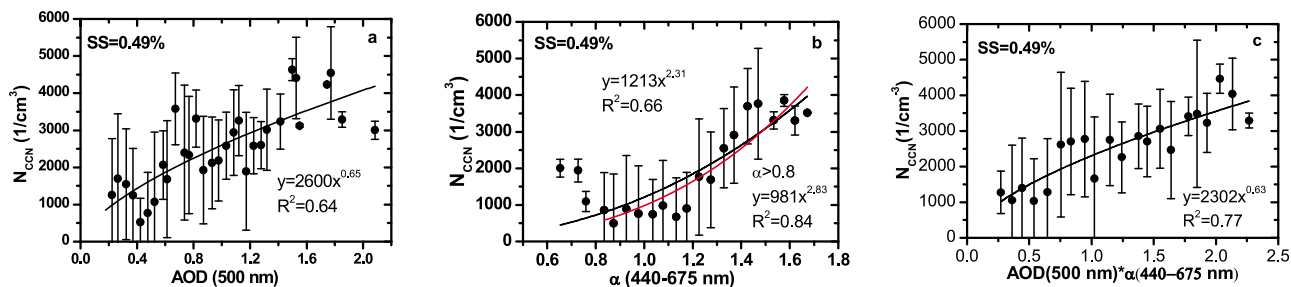

Figure 9. Mean N_{CCN} at 0.49% SS as function of (a) AOD (500 nm), (b) α (440–675 nm, black line for all data and red line for $\alpha > 0.8$) and (c) AOD (500 nm) * α (440–675 nm) during the entire observation period. N_{CCN} is averaged over every 0.1 AOD, 0.1 α and 0.1 AOD * α bin from the lowest values of AOD, α and AOD * α to the highest values of AOD, α and AOD * α. Error bars represent the standard deviation of N_{CCN} in each bin.
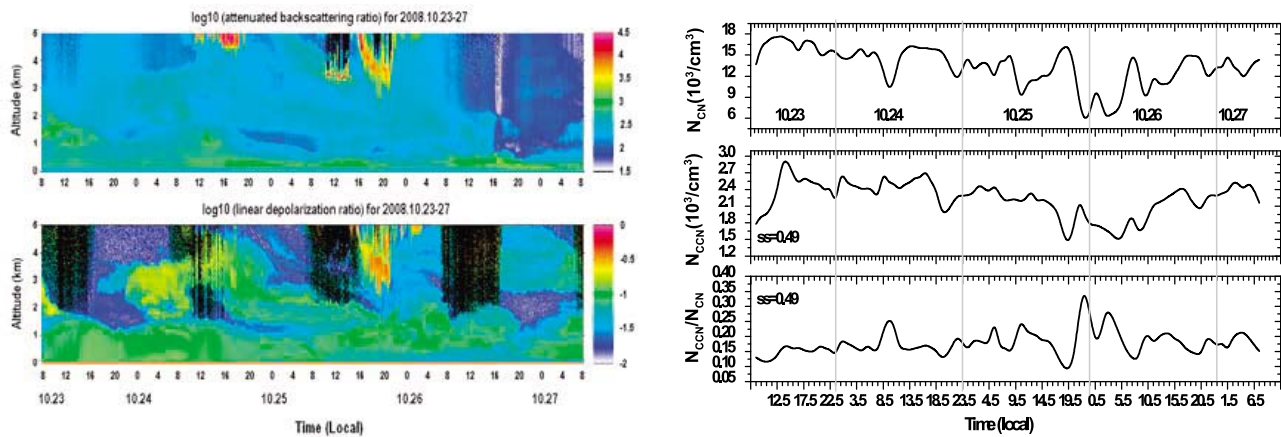
Figure 10. (left) Vertical and temporal distributions of (top) aerosol-attenuated backscattering ratio and (bottom) aerosol linear depolarization ratio from MPL measurements made during a moderate dust event. (right) The corresponding variations in (top) N_{CN}, (middle) N_{CCN} and (bottom) N_{CCN}/N_{CN} at 0.49% SS during the dust event.

Figure 9c shows the mean N_{CCN} (at SS = 0.49%) as a function of AOD (500 nm)* α (440–675 nm) during the entire period. Although there is a large range in CCN concentration at a given AOD*α, the correlation ($R^2 = 0.77$) is better than it was for CCN concentration as a function of AOD ($R^2 = 0.64$) or as a function of α ($R^2 = 0.66$). Previous studies have shown that the columnar aerosol number is proportional to the product of two remotely sensed physical quantities, AOD*α, and that there is a positive correlation between columnar cloud particle number and columnar aerosol particle number [*Nakajima and Nakajima*, 1995; *Nakajima et al.*, 2001].

[29] On the other hand, the large standard deviations imply that it is difficult to describe any correlation between CCN number and aerosol optical properties using a single simple relation because even though related to aerosol loading, the two variables describe different aspects of aerosol properties. More detailed relationships involving more aerosol properties (size and/or composition information) as well as meteorological variables (e.g., relative humidity) should be developed.

3.2.3. CCN During a Moderate Dust Event

[30] MPL depolarization measurements detected a moderate dust event from October 23 to October 27, 2008. Dust aerosols have a larger linear depolarization ratio than other

aerosol types because of the non-sphericity of dust particles. The vertical distribution and spatiotemporal evolution of the aerosol-attenuated backscattering ratio and the aerosol linear depolarization ratio during the dust event is given in Figure 10 (left). A significant dust layer was found below 2 km with a linear depolarization ratio of about 0.1. For a typical dust event in a dust source region, the linear depolarization ratio can be greater than 0.3 [*Gobbi et al.*, 2000]. The relatively small linear depolarization ratios in this aerosol layer suggests that dust aerosols were mixed with anthropogenic pollution aerosols, which are more spherical in shape. The attenuated backscattering ratio and the linear depolarization ratio provide information about the aerosol concentration and the relative amounts of dust aerosols within mixed aerosols near the surface.

[31] Figure 10 (right) shows the variation of N_{CN}, N_{CCN} and N_{CCN}/N_{CN} (SS = 0.49%) during the course of the dust event. The values of N_{CN} are influenced by the aerosol vertical distribution, especially from 21:00 (local time) on October 25 to 5:00 (local time) on October 26, relatively small values of N_{CN} were found. The variation of N_{CCN}, on average, follows that of N_{CN}, although at times, they are negatively correlated. Figure 11 shows the variation of N_{CCN} (left panel) and N_{CCN}/N_{CN} (right panel) (SS = 0.49%)
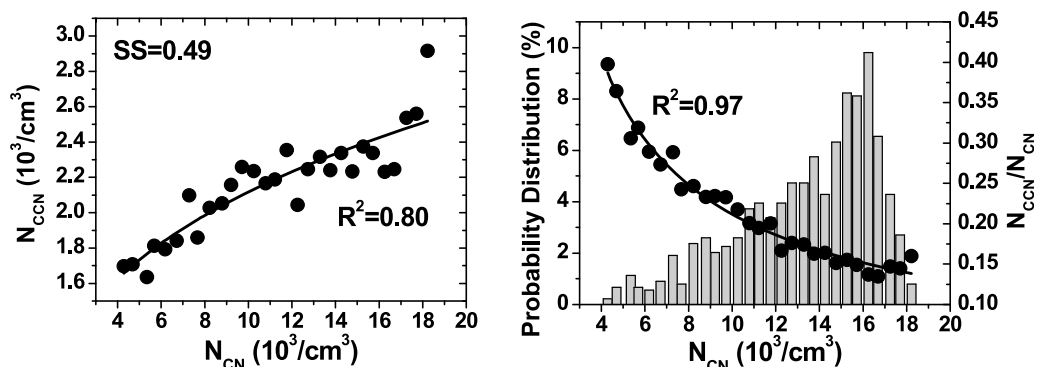

Figure 11. (left and right) N_{CCN} and N_{CCN}/N_{CN} (at 0.49% SS) as function of N_{CN} and (right) the probability distribution of N_{CN} during the dust event.

as a function of N_{CN} during the dust event. Although there is a significant decrease in N_{CCN}/N_{CN} with increasing N_{CN} ($R^2 = 0.97$), N_{CCN} increases with increasing N_{CN}. On the whole, during the dust episode, CN concentrations in excess of 10^4 cm^{-3} were found (Figure 11, right); the mean value was 13392 ± 3168 cm^{-3}, which is significantly larger than the mean value during the entire field campaign. The mean value of N_{CCN} was 2246 ± 536 cm^{-3}, which is much smaller than the mean value for the entire observation period.

[32] The conditions under which dust particles can serve as CCN are currently not well known [*Levin et al.*, 2005; *Kelly et al.*, 2007]. Dust aerosols are primarily composed of insoluble components or components with low solubility, so the ability of dust particles to serve as CCN strongly depends on the presence of minor soluble components [*Rosenfeld et al.*, 2001; *Kelly et al.*, 2007]. However, studies show that during long-range transport or over a long period of evolution, dust particles can become internally mixed with other chemical species through condensation, coagulation, surface chemical reactions, and aqueous phase chemical reactions [*Manktelow et al.*, 2010]. For example, the $CaCO_3$ in dust can react with gases such as HNO_3 to form components such as calcium nitrate, which can deliquesce at low RH levels and greatly enhance dust hygroscopicity [*Laskin et al.*, 2005; *Matsuki et al.*, 2010]. For dust without carbonates, condensation of sulfuric acid could lead to a highly soluble form of sulfate, such as $(NH_4)_2SO_4$, coating the surface of dust particles, and increasing the ability of dust to serve as CCN [*Levin et al.*, 1996; *Kelly et al.*, 2007; *Manktelow et al.*, 2010]. The amount of the soluble material on these dust particles is related to their surface area [*Levin et al.*, 1996]. A simple theory of CCN hygroscopic growth and drop activation on CCN with a thin soluble shell on the dust surface showed that dust with even a very small soluble fraction can be an efficient CCN at not very high supersaturation levels [*Khvorostyanov and Curry*, 2007].

[33] In our study, the significant decrease of N_{CCN}/N_{CN} with increasing CN concentrations and relatively small CCN concentrations indicate that in spite of the existence of mixed dust aerosols with other anthropogenic aerosols, most of the dust aerosol particles are inactive as CCN. The reasons are not very clear, but some studies may provide an explanation. A previous study showed that total CCN over dust source regions either doubled or decreased by as much as 20%, depending on the size distribution of dust emissions [*Lee et al.*, 2009]. Another study on the impact of dust on sulfate aerosols during an East Asian dust storm showed that dust can coagulate and scavenge small nuclei. The uptake of H_2SO_4 vapor and its precursor gas, SO_2, on dust may suppress new sulfate particle formation, and reduce growth by condensation and cloud processing. These effects would reduce total CCN concentrations, although the effect on CCN may be partly compensated or reversed by additional CCN from dust particles internally mixed with soluble material [*Manktelow et al.*, 2010].

4. Summary and Conclusions

[34] CCN and aerosol properties at SS = 0.08–1.37% were measured at one polluted continental site in China (Shouxian in Anhui Province) from August 1–October 31, 2008

during the AMF deployment to study aerosol indirect effects in China. Investigated in this study are the variation in CCN number concentrations and fraction of CCN activation properties, the dependence of CCN and CCN activation properties on meteorological parameters and the relationship between CCN properties and aerosol properties, as well as CCN properties during a moderate dust event.

[35] The magnitudes of N_{CN} and N_{CCN} at SS = 0.49% were large and changed significantly over the course of the field campaign. The range of daily mean N_{CN} was 3095–12014 cm^{-3}, 2315–7416 cm^{-3}, and 4267–15508 cm^{-3} in August, September, and October, respectively, and the range of corresponding daily mean N_{CCN} was 1964–5677 cm^{-3}, 1771–3536 cm^{-3}, and 1526–5706 cm^{-3}. The mean aerosol CCN activation rate (N_{CCN}/N_{CN} at 0.49% SS) was 0.53, which is slightly larger than that reported by other studies made in eastern China. Peaks in the diurnal variation of CN and CCN occurred in the early morning and the late afternoon when human activities were at their maximum.

[36] Close relationships between CCN concentrations, N_{CCN}/N_{CN} ratios and ambient meteorological conditions were found at the Shouxian site. N_{CCN} and N_{CCN}/N_{CN} increased significantly with increasing temperature. CCN were more abundant in the air mass that originated from densely polluted areas and the air mass composed of a mixture of maritime and continental aerosols. The same magnitudes of N_{CN} were found in the continental air that originated from the interior and the polluted air that originated from the western Pacific.

[37] N_{CCN} increased significantly with increasing N_{CN}, but their ratio (N_{CCN}/N_{CN}) decreased with increasing N_{CN} under low SS (<0.49%) conditions, indicating that a greater portion of smaller particles and/or their chemical composition were less favorable for activating as CCN. A test study on the relationship between N_{CCN} and aerosol optical properties showed a correlation between N_{CCN} (at 0.49% SS) and AOD (500 nm), and especially between N_{CCN} (at 0.49% SS) and α (440–675 nm, >0.8). Both relationships can be described using a power law function at this polluted continental site. A stronger relationship between CCN and the product of AOD (500 nm) and α (440–675 nm) was found. These may offer another way to estimate CCN by taking advantage of the wealth of remotely sensed AOD data.

[38] There were obvious responses in the magnitudes of N_{CN}, N_{CCN} and N_{CCN}/N_{CN} to the dust event. On the whole, the moderate dust event identified in this study significantly increased the magnitude of N_{CN} and decreased the ratio N_{CCN}/N_{CN}, implying that dust particles do not increase N_{CCN} much, despite mixing with other anthropogenic aerosols.

References

Abdul-Razzak, H., and S. J. Ghan (2000), A parameterization of aerosol activation: 2. Multiple aerosol types, *J. Geophys. Res.*, *105*, 6837–6844, doi:10.1029/1999JD901161.

Alexandrov, M. D., A. Marshak, B. Cairns, A. A. Lacis, and B. E. Carlson (2004), Automated cloud screening algorithm for MFRSR data, *Geophys. Res. Lett.*, *31*, L04118, doi:10.1029/2003GL019105.

Alexandrov, M. D., A. A. Lacis, B. E. Carlson, and B. Cairns (2008), Characterization of atmospheric aerosols using MFRSR measurements, *J. Geophys. Res.*, *113*, D08204, doi:10.1029/2007JD009388.

Andreae, M. O. (2009), Correlation between cloud condensation nuclei concentration and aerosol optical thickness in remote and polluted regions, *Atmos. Chem. Phys.*, *9*, 543–556, doi:10.5194/acp-9-543-2009.

Asa-Awuku, A., G. J. Engelhart, B. H. Lee, S. N. Pandis, and A. Nenes (2009), Relating CCN activity, volatility, and droplet growth kinetics of β-caryophyllene secondary organic aerosol, *Atmos. Chem. Phys.*, *9*, 795–812, doi:10.5194/acp-9-795-2009.

Campbell, J. R., D. L. Hlavka, E. J. Welton, C. J. Flynn, D. D. Turner, J. D. Spinhirne, V. S. Scott, and I. H. Hwang (2002), Full-time, eye-safe cloud and aerosol lidar observation at atmospheric radiation measurement program sites: Instrument and data processing, *J. Atmos. Oceanic Technol.*, *19*, 431–442, doi:10.1175/1520-0426(2002)019<0431:FTESCA>2.0. CO;2.

Cheng, Y. F., et al. (2008), Relative humidity dependence of aerosol optical properties and direct radiative forcing in the surface boundary layer at Xinken in Pearl River Delta of China: An observation based numerical study, *Atmos. Environ.*, *42*(25), 6373–6397, doi:10.1016/j.atmosenv. 2008.04.009.

Cohard, J. M., J. P. Pinty, and K. Suhre (2000), On the parameterization of activation spectra from cloud condensation nuclei microphysical properties, *J. Geophys. Res.*, *105*(D9), 11,753–11,766, doi:10.1029/ 1999JD901195.

Dubovik, O., and M. King (2000), A flexible inversion algorithm for retrieval of aerosol optical properties from Sun and sky radiance measurements, *J. Geophys. Res.*, *105*, 20,673–20,696, doi:10.1029/ 2000JD900282.

Dusek, U., et al. (2006), Size matters more than chemistry for cloud-nucleating ability of aerosol particles, *Science*, *312*(5778), 1375–1378, doi:10.1126/science.1125261.

Eck, T. F., B. N. Holben, J. S. Reid, O. Dubovik, A. Smirnov, N. T. O'Neill, I. Slutsker, and S. Kinne (1999), Wavelength dependence of the optical depth of biomass burning, urban and desert dust aerosols, *J. Geophys. Res.*, *104*, 31,333–31,349, doi:10.1029/1999JD900923.

Elminir, H. K. (2005), Dependence of urban air pollutants on meteorology, *Sci. Total Environ.*, *350*(1–3), 225–237, doi:10.1016/j.scitotenv. 2005.01.043.

Fan, X., H. Chen, X. Xia, Z. Li, and M. Cribb (2010), Aerosol optical properties from the Atmospheric Radiation Measurement Mobile Facility at Shouxian, China, *J. Geophys. Res.*, *115*, D00K33, doi:10.1029/ 2010JD014650.

Flynn, C. J., A. Mendoza, Y. Zheng, and S. Mathur (2007), Novel polarization-sensitive micropulse lidar measurement technique, *Opt. Express*, *15*(6), 2785–2790, doi:10.1364/OE.15.002785.

Fountoukis, C., and A. Nenes (2005), Continued development of a cloud droplet formation parameterization for global climate models, *J. Geophys. Res.*, *110*, D11212, doi:10.1029/2004JD005591.

Ghana, S., C. Chuang, R. Easter, and J. Penner (1995), A parameterization of cloud droplet nucleation, part II, multiple aerosol types, *Atmos. Res.*, *36*, 39–54, doi:10.1016/0169-8095(94)00005-X.

Gobbi, G. P., F. Barnaba, R. Giorgi, and A. Santacasa (2000), Altitude resolved properties of a Saharan dust event over the Mediterranean, *Atmos. Environ.*, *34*, 5119–5127, doi:10.1016/S1352-2310(00)00194-1.

Gunthe, S., et al. (2009), Cloud condensation nuclei in pristine tropical rainforest air of Amazonia: Size-resolved measurements and modeling of atmospheric aerosol composition and CCN activity, *Atmos. Chem. Phys.*, *9*, 7551–7575, doi:10.5194/acp-9-7551-2009.

Harrison, L., and J. Michalsky (1994), Objective algorithms for the retrieval of optical depths from ground-based measurements, *Appl. Opt.*, *33*, 5126–5132, doi:10.1364/AO.33.005126.

Huang, Y., W. L. Chameides, and R. E. Dickinson (2007), Direct and indirect effects of anthropogenic aerosols on regional precipitation over east Asia, *J. Geophys. Res.*, *112*, D03212, doi:10.1029/2006JD007114.

Hudson, J. G., and X. Da (1996), Volatility and size of cloud condensation nuclei, *J. Geophys. Res.*, *101*(D2), 4435–4442, doi:10.1029/95JD00192.

Hudson, J. G., and S. S. Yum (2002), Cloud condensation nuclei spectra and polluted and clean clouds over the Indian Ocean, *J. Geophys. Res.*, *107*(D19), 8022, doi:10.1029/2001JD000829.

Jefferson, A. (2005), Aerosol Observing System (AOS) Handbook, *ARM TR-014*, 17 pp., U.S. Dep. of Energy, Washington, D. C.

Kelly, J. T., C. C. Chuang, and A. S. Wexler (2007), Influence of dust composition on cloud droplet formation, *Atmos. Environ.*, *41*(14), 2904–2916, doi:10.1016/j.atmosenv.2006.12.008.

Khvorostyanov, V. I., and J. A. Curry (2006), Aerosol size spectra and CCN activity spectra: Reconciling the lognormal, algebraic, and power laws, *J. Geophys. Res.*, *111*, D12202, doi:10.1029/2005JD006532.

Khvorostyanov, V. I., and J. A. Curry (2007), Refinements to the Köhler's theory of aerosol equilibrium radii, size spectra, and droplet activation: Effects of humidity and insoluble fraction, *J. Geophys. Res.*, *112*, D05206, doi:10.1029/2006JD007672.

Khvorostyanov, V. I., and J. A. Curry (2008), Kinetics of cloud drop formation and its parameterization for cloud and climate models, *J. Atmos. Sci.*, *65*, 2784–2802, doi:10.1175/2008JAS2606.1.

Khvorostyanov, V. I., and J. A. Curry (2009), Parameterization of cloud drop activation based on analytical asymptotic solutions to the supersaturation equation, *J. Atmos. Sci.*, *66*, 1905–1925, doi:10.1175/ 2009JAS2811.1.

Kuang, C., P. H. McMurry, and A. V. McCormick (2009), Determination of cloud condensation nuclei production from measured new particle formation events, *Geophys. Res. Lett.*, *36*, L09822, doi:10.1029/ 2009GL037584.

Laskin, A., T. W. Wietsma, B. J. Krueger, and V. H. Grassian (2005), Heterogeneous chemistry of individual mineral dust particles with nitric acid: A combined CCSEM/EDX, ESEM, and ICPMS study, *J. Geophys. Res.*, *110*, D10208, doi:10.1029/2004JD005206.

Lau, K.-M., et al. (2008), The joint aerosol monsoon experiment: A new challenge for monsoon climate research, *Bull. Am. Meteorol. Soc.*, *89*, doi:10.1175/BAMS-89-3-369.

Lee, K.-H., Z. Li, M. Cribb, J. Liu, L. Wang, Y. Zheng, X. Xia, H. Chen, and B. Li (2010), Aerosol optical depth measurements in eastern China and a new calibration method, *J. Geophys. Res.*, *115*, D00K11, doi:10.1029/2009JD012812.

Lee, Y. H., K. Chen, and P. J. Adams (2009), Development of a global model of mineral dust aerosol microphysics, *Atmos. Chem. Phys.*, *9*, 2441–2458, doi:10.5194/acp-9-2441-2009.

Levin, Z., E. Ganor, and V. Gladstein (1996), The effects of desert particles coated with sulfate on rain formation in the Eastern Mediterranean, *J. Appl. Meteorol.*, *35*, 1511–1523, doi:10.1175/1520-0450(1996)035<1511: TEODPC>2.0.CO;2.

Levin, Z., A. Teller, E. Ganor, and Y. Yin (2005), On the interactions of mineral dust, sea-salt particles, and clouds: A measurement and modeling study from the Mediterranean Israeli Dust Experiment campaign, *J. Geophys. Res.*, *110*, D20202, doi:10.1029/2005JD005810.

Li, Z., et al. (2007a), Preface to special section on East Asian Studies of Tropospheric Aerosols: An International Regional Experiment (EAST-AIRE), *J. Geophys. Res.*, *112*, D22S00, doi:10.1029/2007JD008853.

Li, Z., et al. (2007b), Aerosol optical properties and their radiative effects in northern China, *J. Geophys. Res.*, *112*, D22S01, doi:10.1029/ 2006JD007382.

Li, Z., et al. (2011), East Asian Studies of Tropospheric Aerosols and Impact on Regional Climate (EAST-AIRC): An overview, *J. Geophys. Res.*, *116*, D00K34, doi:10.1029/2010JD015257.

Manktelow, P. T., K. S. Carslaw, G. W. Mann, and D. V. Spracklen (2010), The impact of dust on sulfate aerosol, CN and CCN during an East Asian dust storm, *Atmos. Chem. Phys.*, *10*(2), 365–382, doi:10.5194/acp-10-365-2010.

Martins, J. A., et al. (2009), Cloud condensation nuclei from biomass burning during the Amazonian dry-to-wet transition season, *Meteorol. Atmos. Phys.*, *104*(1–2), 83–93, doi:10.1007/s00703-009-0019-6.

Matsuki, A., A. Schwarzenboeck, H. Venzac, P. Lai, S. Crumeyrolle, and L. Gomes (2010), Cloud processing of mineral dust: Direct comparison of cloud residual and clear sky particles during AMMA aircraft campaign in summer 2006, *Atmos. Chem. Phys.*, *10*(3), 1057–1069, doi:10.5194/ acp-10-1057-2010.

Nakajima, T. Y., and T. Nakajima (1995), Wide-area determination of cloud microphysical properties from NOAA AVHRR measurements for FIRE and ASTEX regions, *J. Atmos. Sci.*, *52*, 4043–4059, doi:10.1175/1520-0469(1995)052<4043:WADOCM>2.0.CO;2.

Nakajima, T., A. Higurashi, K. Kawamoto, and J. E. Penner (2001), A possible correlation between satellite derived cloud and aerosol microphysical parameters, *Geophys. Res. Lett.*, *28*(7), 1171–1174, doi:10.1029/ 2000GL012186.

Nicolás, J. F., E. Yubero, C. Pastor, J. Crespo, and A. Carratalá (2009), Influence of meteorological variability upon aerosol mass size distribution, *Atmos. Res.*, *94*(2), 330–337, doi:10.1016/j.atmosres.2009.06.007.

Oshima, N., M. Koike, Y. Zhang, and Y. Kondo (2009), Aging of black carbon in outflow from anthropogenic sources using a mixing state resolved model: 2. Aerosol optical properties and cloud condensation nuclei activities, *J. Geophys. Res.*, *114*, D18202, doi:10.1029/ 2008JD011681.

Rissman, T. A., T. M. VanReken, J. Wang, R. Gasparini, D. R. Collins, H. H. Jonsson, F. J. Brechtel, R. C. Flagan, and J. H. Seinfeld (2006),

Characterization of ambient aerosol from measurements of cloud condensation nuclei during the 2003 Atmospheric Radiation Measurement Aerosol Intensive Observational Period at the Southern Great Plains site in Oklahoma, *J. Geophys. Res.*, *111*, D05S11, doi:10.1029/2004JD005695.

Roberts, G. C., and A. Nenes (2005), A continuous-flow streamwise thermal-gradient CCN chamber for atmospheric measurements, *Aerosol Sci. Technol.*, *39*, 206–221, doi:10.1080/027868290913988.

Rose, D., A. Nowak, P. Achtert, A. Wiedensohler, M. Hu, M. Shao, Y. Zhang, M. O. Andreae, and U. Pöschl (2008), Cloud condensation nuclei in polluted air and biomass burning smoke near the mega-city Guangzhou, China–Part 1: Size-resolved measurements and implications for the modeling of aerosol particle hygroscopicity and CCN activity, *Atmos. Chem. Phys. Discuss.*, *8*, 17,343–17,392, doi:10.5194/acpd-8-17343-2008.

Rosenfeld, D., Y. Rudich, and R. Lahav (2001), Desert dust suppressing precipitation: A possible desertification feedback loop, *Proc. Natl. Acad. Sci. U. S. A.*, *98*(11), 5975–5980, doi:10.1073/pnas.101122798.

Rosenfeld, D., J. Dai, X. Yu, Z. Yao, X. Xu, X. Yang, and C. Du (2007), Inverse relations between amounts of air pollution and orographic precipitation, *Science*, *315*(5817), 1396–1398, doi:10.1126/science.1137949.

Ross, K. E., S. J. Piketh, R. T. Bruintjes, R. P. Burger, R. J. Swap, and H. J. Annegarn (2003), Spatial and seasonal variations in CCN distribution and the aerosol-CCN relationship over southern Africa, *J. Geophys. Res.*, *108*(D13), 8481, doi:10.1029/2002JD002384.

Saleeby, S. M., and W. R. Cotton (2004), A large-droplet mode and prognostic number concentration of cloud droplets in the Colorado State Univ. Regional Atmospheric Modeling System (RAMS). Part I: Module descriptions and supercell test simulations, *J. Appl. Meteorol.*, *43*(1), 182–195, doi:10.1175/1520-0450(2004)043<0182:ALMAPN>2.0.CO;2.

Streets, D. G., C. Yu, Y. Wu, M. Chin, Z. Zhao, T. Hayasaka, and G. Shi (2008), Aerosol trends over China, 1980–2000, *Atmos. Res.*, *88*, 174–182, doi:10.1016/j.atmosres.2007.10.016.

Twomey, S. (1974), Pollution and planetary albedo, *Atmos. Environ.*, *8*, 1251–1256, doi:10.1016/0004-6981(74)90004-3.

Welton, E. J., K. J. Voss, P. K. Quinn, P. J. Flatau, K. Markowicz, J. R. Campbell, J. D. Spinhirne, H. R. Gordon, and J. E. Johnson (2002), Measurements of aerosol vertical profiles and optical properties during INDOEX 1999 using micro-pulse lidars, *J. Geophys. Res.*, *107*(D19), 8019, doi:10.1029/2000JD000038.

Xia, X., Z. Li, B. Holben, P. Wang, T. Eck, H. Chen, M. Cribb, and Y. Zhao (2007), Aerosol optical properties and radiative effects in the Yangtze Delta region of China, *J. Geophys. Res.*, *112*, D22S12, doi:10.1029/2007JD008859.

Xin, J., et al. (2007), AOD and Angstrom exponent of aerosols observed by the Chinese Sun Hazemeter Network from August 2004 to September 2005, *J. Geophys. Res.*, *112*, D05203, doi:10.1029/2006JD007075.

Xu, Q. (2001), Abrupt change of the mid-summer climate in central east China by the influence of atmospheric pollution, *Atmos. Environ.*, *35*, 5029–5040, doi:10.1016/S1352-2310(01)00315-6.

Yum, S. S., and J. G. Hudson (2001), Vertical distributions of cloud condensation nuclei spectra over the springtime Arctic Ocean, *J. Geophys. Res.*, *106*(D14), 15,045–15,052, doi:10.1029/2000JD900357.

Yum, S. S., J. G. Hudson, K. Y. Song, and B. C. Choi (2005), Springtime cloud condensation nuclei concentrations on the west coast of Korea, *Geophys. Res. Lett.*, *32*, L09814, doi:10.1029/2005GL022641.

Yum, S. S., G. Roberts, J. H. Kim, K. Song, and D. Kim (2007), Submicron aerosol size distributions and cloud condensation nuclei concentrations measured at Gosan, Korea, during the Atmospheric Brown Clouds–East Asian Regional Experiment 2005, *J. Geophys. Res.*, *112*, D22S32, doi:10.1029/2006JD008212.

Zhang, R., G. Li, J. Fan, D. L. Wu, and M. J. Molina (2007), Intensification of Pacific storm track linked to Asian pollution, *Proc. Natl. Acad. Sci. U. S. A.*, *104*, 5295–5299, doi:10.1073/pnas.0700618104.

M. Cribb and Z. Li, Department of Atmospheric and Oceanic Science and Earth System Science Interdisciplinary Center, University of Maryland, College Park, 5825 University Research Ct., Ste. 4001, College Park, MD 20742, USA. (zli@atmos.umd.edu)

J. Liu and Y. Zheng, Jiangsu Key Laboratory of Atmospheric Environment Monitoring and Pollution Control, Nanjing University of Information Science and Technology, Nanjing 210044, China.